Progress In Electromagnetics Research, Vol. 117, 209–236, 2011

EVALUATION OF ELECTROMAGNETIC FIELDS ASSOCIATED WITH INCLINED LIGHTNING CHANNEL USING SECOND ORDER FDTD-HYBRID METHODS

M. Izadi*, M. Z. A. A. Kadir, and C. Gomes

Centre of Excellence on Lightning Protection (CELP), Faculty of Engineering, University Putra Malaysia, UPM, Serdang, Selangor 43400, Malaysia

Abstract—Evaluation of electromagnetic fields caused by the lightning channel is an appealing topic in order to consider the indirect effects of lightning on the power lines. A common assumption for the calculation of electromagnetic fields at the observation point is a vertical lightning channel, but the fact is that in reality the lightning channel is seldom vertical on the ground surface. In this study, the electromagnetic fields due to inclined lightning channel at various observation points with different angles and with respect to the image of lightning channel on the ground surface were explored. This study also proposes general equations that can estimate the electric fields due to inclined lightning channel through the 2nd FDTD method. The proposed method supports the notion of vertical lightning channel while the channel angle with respect to z-axis is assumed to be zero. This method was validated through the data gathered from five fields: three at a close distance from inclined lightning channel and two at intermediate distances from vertical lightning channel. Similarly, due to inclined lightning channel, the effects of geometrical and current parameters on the electromagnetic fields are considered. This study substantiates different coupling models with FDTD structure directly at the time domain without a need for extra converters.

1. INTRODUCTION

One of the appealing areas under discussion is the electromagnetic fields due to lightning channel in order to appoint proper protection level on the power lines and equipments while the electromagnetic

Received 21 April 2011, Accepted 17 May 2011, Scheduled 6 June 2011

* Corresponding author: Mahdi Izadi (aryaphase@yahoo.com).

fields is one of the most influential factors in creating induction voltage on the power lines [1]. Several studies have been done on the evaluation of electromagnetic fields due to lightning channel with the assumption that the lightning channel strikes the ground at a vertical angle [2]. However, it is known to be tortuous on scales ranging from less than 1 m to over 1 km [3–5]. Moreover, the lightning channel typically strikes the ground at an angle less than ninety degrees (with respect to the ground) [6]. Several studies on the radiated electromagnetic fields associated with inclined and tortuosity lightning channels have been done while generally the tortuosity lightning channel is modeled with some individual linear inclined channel segments [3, 5, 7, 8]. Accordingly, this paper focuses on the computation of the electromagnetic fields due to the inclined lightning channel at the observation point in the time domain using second order FDTD (later referred as 2nd FDTD) Hybrid method. The method is then validated by the data collected from three fields stricken by lightning at a close distance from the inclined lightning channel whereas the channel angle (between lightning channel and z-axis) can be determined by a high speed camera [6]. In addition, the effects of the channel angel and observation point angle (between the vector from channel base to image of observation point on the ground and the image of lightning channel on the ground surface) on the electromagnetic field values are evaluated. The results due to inclined channel are compared with the field values associated with the vertical channel. Also, the proposed method is validated for vertical lightning channel where the channel angle is equal to zero. The three fundamental assumptions in this study are:

(i) The ground conductivity is perfect

(ii) The lightning channel is without any branches

(iii) The current velocity along lightning channel is constant

For the simulation of electromagnetic fields due to lightning channel, it is necessary to consider both the return stroke current at the channel base and the lightning channel in a special function and a current model, respectively. In this study, the channel base current is simulated by the DU function [9] which is an improved function of Heidler's function [10] and is in agreement with the measured current at the channel base. The engineering models are used in this simulator, since the return stroke currents at different heights along with lightning channel are generally expressed by a special function based on the channel base current and a height dependent attenuation factor in these models.

2. RETURN STROKE CURRENT

As mentioned earlier, the channel base current in this study is simulated by the DU function which can be expressed by Equation (1) [9]

$$i\,(0,t)=\left[\frac{i_{01}}{\eta_1}\frac{\left(\frac{t}{\Gamma_{11}}\right)^{n_1}}{1+\left(\frac{t}{\Gamma_{11}}\right)^{n_1}}\exp\left(\frac{-t}{\Gamma_{12}}\right)+\frac{i_{02}}{\eta_2}\frac{\left(\frac{t}{\Gamma_{21}}\right)^{n_2}}{1+\left(\frac{t}{\Gamma_{21}}\right)^{n_2}}\exp\left(\frac{-t}{\Gamma_{22}}\right)\right] \tag{1}$$

where
$i_{01},\ i_{02}$ are the amplitudes of the channel base current,
$\Gamma_{11},\ \Gamma_{12}$ are the front time constants,
$\Gamma_{21},\ \Gamma_{22}$ are the decay-time constants,
$n_1,\ n_2$ are the exponents $(2 \sim 10)$,

$$\eta_1 = \exp\left[-\left(\Gamma_{11}/\Gamma_{12}\right)\left(n_1 \times \frac{\Gamma_{12}}{\Gamma_{11}}\right)^{\frac{1}{n_1}}\right],$$

$$\eta_2 = \exp\left[-\left(\Gamma_{21}\Gamma_{22}\right)\left(n_2 \times \frac{\Gamma_{22}}{\Gamma_{21}}\right)^{\frac{1}{n_2}}\right]$$

For instance, the measured channel bases current from a triggered lightning experiment in Florida is illustrated in Figure 1. The channel base current parameters using DU function with respect to measured current are estimated while the numerical fitting method is applied; the results are tabulated in Table 1.

A simulation of the channel base current using initial current parameters from Table 1 is shown in Figure 2.

In this study, the current wave shape along with the lightning channel is predicted by the engineering return stroke current models,

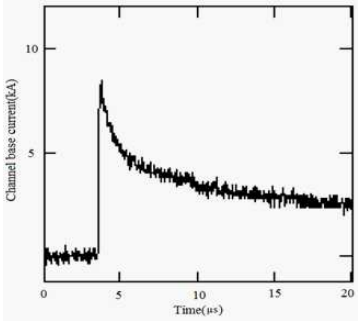

Figure 1. The measured return stroke current at channel bases from triggered lightning experiment [6].

Table 1. Typical values for Diendorfer and Uman channel base current function.

$\mathbf{i_{01}}$ (A)	$\mathbf{i_{02}}$ (A)	$\mathbf{\Gamma_{11}}$ (s)	$\mathbf{\Gamma_{12}}$ (s)	$\mathbf{\Gamma_{21}}$ (s)	$\mathbf{\Gamma_{22}}$ (s)	$\mathbf{n_1}$	$\mathbf{n_2}$
8×10^3	3.6671×10^3	9.5×10^{-8}	8.5×10^{-7}	1.4×10^{-6}	1.8×10^{-5}	2	2

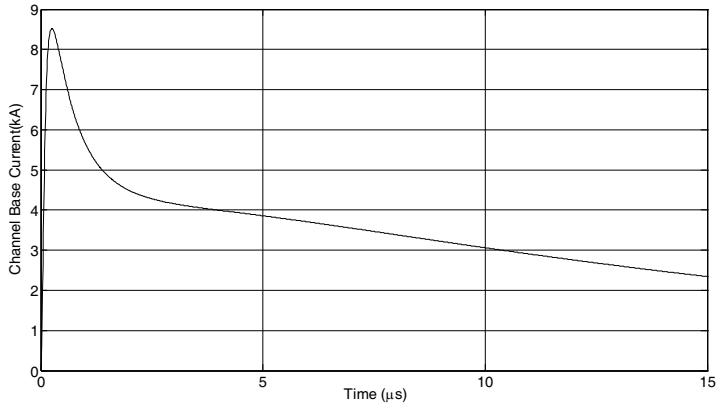

Figure 2. The simulated channel base current using DU function based on current parameters from Table 1.

Table 2. $P(z')$ and v for five engineering models based on Equation (2) [3].

Model	$P(z')$	v
BG	1	∞
TCS	1	$-c$
TL	1	v_f
MTLL	$(1-\frac{z'}{H})$	v_f
MTLE	$\exp(-\frac{z'}{\lambda})$	v_f

while the focus is on the current by a special function that depends on channel base current and a height dependent attenuation factor. The engineering models can usually be presented by a general equation such as Equation (2). The most common applied engineering models are namely the Bruce-Golde model (BG) [11], Traveling Current Source model (TCS) [12], Transmission Line model (TL) [2], Modified Transmission Line Linear model with Linear decay with height (MTLL) [2], Modified Transmission Line model with Exponential decay with height (MTL) or (MTLE) [2]. Theses models are tabulated

in Table 2 based on the current parameters in Equation (2) [3, 13] where λ is the decay constant ($\sim 2\,\text{km}$) and H is the cloud's height.

$$I\left(z',t\right) = I\left(0, t-\frac{z'}{v}\right) \times P\left(z'\right) \times u\left(t-\frac{z'}{v_f}\right) \tag{2}$$

where:
z' is the temporary charge height along the lightning channel,
$I(z',t)$ is the current distribution along the lightning channel at any height z' and any time t,
$I(0,t)$ is the channel base current;
$P(z')$ is the height dependent attenuation factor,
v is the velocity of charge(return stroke current velocity),
v_f is the velocity of return stroke front,
u is the Heaviside function defended as

$$u\left(t-\frac{z'}{v_f}\right) = \begin{cases} 1 & \text{for } t \geq \frac{z'}{v_f} \\ 0 & \text{for } t < \frac{z'}{v_f} \end{cases}$$

There are some drawbacks regarding these models. For instance, the BG and TCS models are not convenient, due to the discontinuity at current [2]. Whilst the TL model is not a complete model because it is not considered on the removed charge along the lightning channel [2, 14]. This model was later modified by the MTLL and MTLE models. In the MTLL and MTLE models, some charges are removed from channel with linear cloud height dependent factor and exponentially rate, respectively [2, 14] This study opted for MTLE model because of the channel height value is considered as unmeasured parameter while the value of λ is recommended around 2 km. In addition, It should be highly remarked that the return stroke velocity is less than light speed in the free space (c) and is typically assumed to be between ($c/3$) to ($2c/3$) [15] the return stroke current wave shape at two different heights with respect to the ground surface along the channel using TL, MTLE and MTLL models are shown in Figure 3 where the channel base current parameters are applied from Table 2. Note that, the λ and H factors are set on 2000 m and 7000 m for MTLE and MTLL models respectively while the return stroke velocity is fixed at 1.3×10^8 m/s.

3. ELECTROMAGNETIC FIELDS DUE TO LIGHTNING CHANNEL

Dipole method which is given in Equations (3) to (5) can be used to show the electromagnetic fields due to vertical lightning channel;

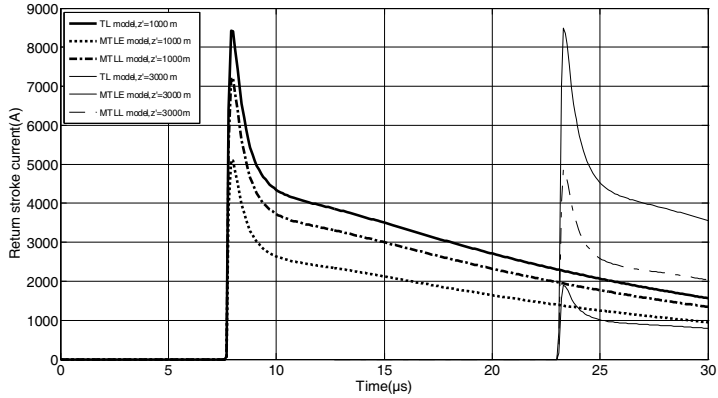

Figure 3. The return stroke current wave shape at different heights along lightning channel using TL, MTLE and MTLL models.

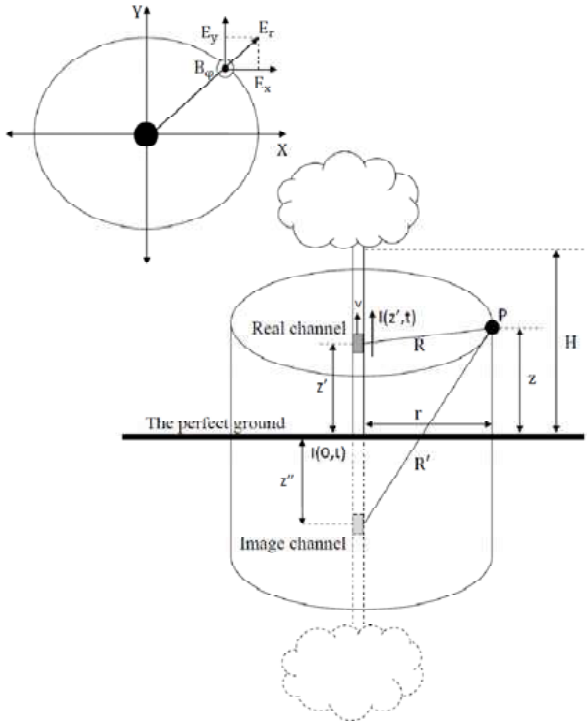

Figure 4. The geometry of the vertical lightning channel.

while the geometry of problem is illustrated in Figure 4 (the ground is assumed to be perfect) [2, 16, 17]

$$\vec{E_r}(r,z,t) = \left(\frac{1}{4\pi\varepsilon_0}\right)\int_{H_2}^{H_1}\left(\frac{3r(z-z')}{R^5}\int_0^t i\left(z',\tau-\frac{R}{c}\right)d\tau + \frac{3r(z-z')}{cR^4}i\left(z',t-\frac{R}{c}\right)+\frac{r(z-z')}{c^2R^3}\frac{\partial i\left(z',t-\frac{R}{c}\right)}{\partial t}\right)dz' \quad (3)$$

$$\vec{E_z}(r,z,t) = \left(\frac{1}{4\pi\varepsilon_0}\right)\int_{H_2}^{H_1}\left(\frac{2(z-z')^2-r^2}{R^5}\int_0^t i\left(z',\tau-\frac{R}{c}\right)d\tau + \frac{2(z-z')^2-r^2}{cR^4}i\left(z',t-\frac{R}{c}\right)-\frac{r^2}{c^2R^3}\frac{\partial i\left(z',t-\frac{R}{c}\right)}{\partial t}\right)dz' \quad (4)$$

$$\vec{B_\varphi}(r,z,t) = \left(\frac{\mu_0}{4\pi}\right)\int_{H_2}^{H_1}\left(\frac{r}{R^3}i\left(z',t-\frac{R}{c}\right)+\frac{r}{cR^2}\frac{\partial i\left(z',t-\frac{R}{c}\right)}{\partial t}\right)dz' \quad (5)$$

where

$R = \sqrt{r^2+(z-z')^2}$,

$R' = \sqrt{r^2+(z+z')^2}$,

$\vec{E_r}(r,z,t)$ is the horizontal electric field due to vertical lightning channel,

$\vec{E_z}(r,z,t)$ is the vertical electric field due to vertical lightning channel,

$\vec{B_\varphi}(r,z,t)$ is the magnetic flux density due to vertical lightning channel,

z is height of observation point,

z' is the vertical space variable,

ε_0 is the permittivity of free space,

μ_0 is the permeability of free space,

$\beta = \frac{v}{c}$,

$H_1 = z' = \frac{\beta}{1-\beta^2}\left\{-(\beta z - ct) - \sqrt{(\beta ct - z)^2 + (r\sqrt{1-\beta^2})^2}\right\}$,

$H_2 = z'' = \frac{\beta}{1-\beta^2}\left\{-(\beta z + ct) + \sqrt{(\beta ct + z)^2 + (r\sqrt{1-\beta^2})^2}\right\}$.

The different components of electric field associated with the lightning channel at a remote observation point can be estimated by the 2nd FDTD-Hybrid method as presented by Equations (6) to (8) and the magnetic flux density can be calculated by Equation (5) [16]. It should be noted that, the observation point is held constant at $(m\Delta y, n\Delta x, p\Delta z)$, the lightning channel is along z-axis and the

processing time is equal to $k\Delta t$

$$\vec{E}_y^k(m,n,p) = \frac{-\varepsilon_0}{\sigma+\frac{3\varepsilon_0}{2\Delta t}}\left\{\frac{\vec{E}_y^{k-2}(m,n,p)-4\vec{E}_y^{k-1}(m,n,p)}{2\Delta t} + \frac{\cos\gamma_1}{\varepsilon_0\mu_0}\left(\frac{\vec{B}_\varphi^k(m,n,p+1)-\vec{B}_\varphi^k(m,n,p-1)}{2\Delta z}\right)\right\} \quad (6)$$

$$\vec{E}_x^k(m,n,p) = \frac{-\varepsilon_0}{\sigma+\frac{3\varepsilon_0}{2\Delta t}}\left\{\frac{\vec{E}_x^{k-2}(m,n,p)-4\vec{E}_x^{k-1}(m,n,p)}{2\Delta t} - \frac{\sin\gamma_1}{\varepsilon_0\mu_0}\left(\frac{\vec{B}_\varphi^k(m,n,p+1)-\vec{B}_\varphi^k(m,n,p-1)}{2\Delta z}\right)\right\} \quad (7)$$

$$\vec{E}_z^k(m,n,p) = \frac{-\varepsilon_0}{\sigma+\frac{3\varepsilon_0}{2\Delta t}}\left\{\frac{\vec{E}_z^{k-2}(m,n,p)-4\vec{E}_z^{k-1}(m,n,p)}{2\Delta t} - \frac{1}{\varepsilon_0\mu_0}\left(\frac{\cos\gamma_3\vec{B}_\varphi^k(m+1,n,p)-\cos\gamma_4\vec{B}_\varphi^k(m-1,n,p)}{2\Delta y} - \frac{-\sin\gamma_5\vec{B}_\varphi^k(m,n+1,p)+\sin\gamma_6\vec{B}_\varphi^k(m,n-1,p)}{2\Delta x}\right)\right\} \quad (8)$$

where σ is the medium conductivity,

$$\cos\gamma_1 = \frac{m\Delta y}{\sqrt{(m\Delta y)^2+(n\Delta x)^2}}$$

$$\sin\gamma_2 = \frac{n\Delta x}{\sqrt{(m\Delta y)^2+(n\Delta x)^2}}$$

$$\cos\gamma_3 = \frac{(m+1)\Delta y}{\sqrt{((m+1)\Delta y)^2+(n\Delta x)^2}}$$

$$\cos\gamma_4 = \frac{(m-1)\Delta y}{\sqrt{((m-1)\Delta y)^2+(n\Delta x)^2}}$$

$$\sin\gamma_5 = \frac{(n+1)\Delta x}{\sqrt{(m\Delta y)^2+((n+1)\Delta x)^2}}$$

$$\sin\gamma_6 = \frac{(n-1)\Delta x}{\sqrt{(m\Delta y)^2+((n-1)\Delta x)^2}}$$

The geometry of problem for estimation of electromagnetic fields due to inclined lightning channel is shown in Figure 6, with the assumption that the lightning channel usually strikes the ground surface with an inclined shape as depicted in Figure 5. The angle between lightning channel and z-axis is illustrated by θ and is called channel angle (see Figure 6) Besides the observation point is located above the ground surface with special angle between the vector from channel base to image of observation point on the ground ($\vec{r}$) and the image of lightning channel on the ground surface (y-axis).

Having applied Maxwell's equations [19] and Lorentz's gauge [20], different components of magnetic flux density in the Cartesian coordinate can be estimated by Equations (9) to (11) which is shown in Figure 6. Note that, the equations of (9) to (11) could easily be solved using Gauss-Lobatto quadrature method [21].

$$\vec{B}_x(x,y,z,\theta,t) = 10^{-7}\times \int_{\frac{H_2}{\cos\theta}}^{\frac{H_1}{\cos\theta}} \left\{ -\cos\theta \left[\frac{y-r'\sin\theta}{cR\left(r'\right)^2} \frac{\partial i\left(r', t-\frac{R(r')}{c}\right)}{\partial t} + \frac{y-r'\sin\theta}{R\left(r'\right)^3} i\left(r', t-\frac{R\left(r'\right)}{c}\right) \right] + \sin\theta \left[\frac{z-r'\cos\theta}{cR\left(r'\right)^2} \frac{\partial i\left(r', t-\frac{R(r')}{c}\right)}{\partial t} + \frac{z-r'\cos\theta}{R\left(r'\right)^3} i\left(r', t-\frac{R\left(r'\right)}{c}\right) \right] \right\} dr' \quad (9)$$

$$\vec{B}_y(x,y,z,\theta,t) = 10^{-7}\times \cos\theta \int_{\frac{H_2}{\cos\theta}}^{\frac{H_1}{\cos\theta}} \left\{ \frac{x}{cR\left(r'\right)^2} \frac{\partial i\left(r', t-\frac{R(r')}{c}\right)}{\partial t} + \frac{x}{R\left(r'\right)^3} i\left(r', t-\frac{R\left(r'\right)}{c}\right) \right\} dr' \quad (10)$$

Figure 5. The video frame for the return stroke lightning channel during the triggered lightning experiment [18].

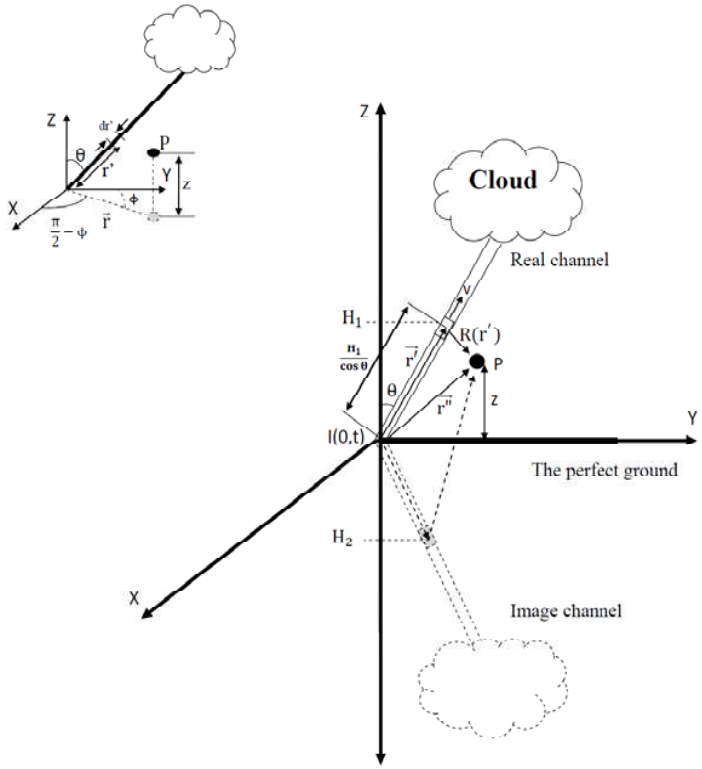

Figure 6. The geometry of the inclined lightning channel with an observation point above the ground surface.

$$\vec{B}_z(x,y,z,\theta,t) = -10^{-7}\times \sin\theta \int_{\frac{H_2}{\cos\theta}}^{\frac{H_1}{\cos\theta}} \left\{ \frac{x}{cR\,(r')^2} \frac{\partial i\left(r', t-\frac{R(r')}{c}\right)}{\partial t} + \frac{x}{R\,(r')^3} i\left(r', t-\frac{R\,(r')}{c}\right) \right\} dr' \qquad (11)$$

where:
r is radial distance from channel base to image of observation point on the ground surface ($r = \sqrt{x^2+y^2}$),
r' is the temporary channel length along lightning channel,
θ is the angle between lightning channel and z axis (the channel angle),
ϕ is the angle between y-axis and $\vec{r}$ while y-axis is fixed on the image of lightning channel on the ground surface (the observation point angle),
x is the position of observation point at x axis ($x = r\sin\phi$),

y is the position of observation point at y axis ($y = r\cos\phi$),
z is observation point height from ground surface,
$\vec{B}_x(x, y, z, \theta, t)$ is the magnetic flux density at x-direction due to inclined lightning channel,
$\vec{B}_y(x, y, z, \theta, t)$ is the magnetic flux density at y-direction due to inclined lightning channel,
$\vec{B}_z(x, y, z, \theta, t)$ is the magnetic flux density at z-direction due to inclined lightning channel.
$R(r') = |\vec{r''} - \vec{r'}| = \sqrt{x^2 + (y - r'\sin\theta)^2 + (z - r'\cos\theta)^2}$.
In addition, the magnetic flux density components in the cylindrical domain can be estimated by Equations (12) to (14)

$$\begin{aligned}
\vec{B}_r(r, z, \phi, \theta, t) &= \cos\left(\frac{\pi}{2} - \phi\right)\vec{B}_x(x, y, z, \theta, t) \\
&\quad + \sin\left(\frac{\pi}{2} - \phi\right)\vec{B}_y(x, y, z, \theta, t) \qquad (12) \\
\vec{B}_\varphi(r, z, \phi, \theta, t) &= -\sin\left(\frac{\pi}{2} - \phi\right)\vec{B}_x(x, y, z, \theta, t) \\
&\quad + \cos\left(\frac{\pi}{2} - \phi\right)\vec{B}_y(x, y, z, \theta, t) \qquad (13) \\
\vec{B}_z(r, z, \phi, \theta, t) &= \vec{B}_z(x, y, z, \theta, t) \qquad (14)
\end{aligned}$$

where:
$\vec{B}_r(r, z, \phi, \theta, t)$ is the magnetic flux density at r-direction due to inclined lightning channel,
$\vec{B}_\varphi(r, z, \phi, \theta, t)$ is the magnetic flux density at φ-direction due to inclined lightning channel,
$\vec{B}_z(r, z, \phi, \theta, t)$ is the magnetic flux density at z-direction due to inclined lightning channel,
$\phi = \arccos\left(\frac{y}{\sqrt{x^2+y^2}}\right)$
The magnetic flux density could also be expressed by Equation (15) regarding Maxwell's equations [16].

$$\nabla \times \vec{B} = \mu_0\left(j + \frac{\partial \vec{D}}{\partial t}\right) = \mu_0\left(\sigma\vec{E} + \varepsilon_0\frac{\partial \vec{E}}{\partial t}\right) \qquad (15)$$

where:
$\vec{J}$ is the current density,
$\vec{D}$ is the electric flux density.

The solutions to curl function in Equation (15) in the Cartesian

coordinates can be presented by Equations (16) to (18) [22]

$$\frac{\partial \vec{E}_x}{\partial t} = \frac{1}{\varepsilon_0 \mu_0}\left(\frac{\partial \vec{B}_z}{\partial y} - \frac{\partial \vec{B}_y}{\partial z} - \mu_0 \sigma \vec{E}_x\right) \tag{16}$$

$$\frac{\partial \vec{E}_y}{\partial t} = \frac{1}{\varepsilon_0 \mu_0}\left(\frac{\partial \vec{B}_x}{\partial z} - \frac{\partial \vec{B}_z}{\partial x} - \mu_0 \sigma \vec{E}_y\right) \tag{17}$$

$$\frac{\partial \vec{E}_z}{\partial t} = \frac{1}{\varepsilon_0 \mu_0}\left(\frac{\partial \vec{B}_y}{\partial x} - \frac{\partial \vec{B}_x}{\partial y} - \mu_0 \sigma \vec{E}_z\right) \tag{18}$$

Therefore, by solving Equations (16) to (18) based on 2nd FDTD method [22–24] and applying perfect ground conductivity conditions, different components of electric field can be expressed by Equations (19) to (21) At the same time, the components of magnetic flux density are obtained from Equations (9) to (11) and the electric fields components in the cylindrical coordinates from Equations (22) to (24)

$$\vec{E}_x(x,y,z,\theta,t_k) = \frac{2\Delta t}{3\varepsilon_0\mu_0}\left(\frac{\vec{B}_z(x,y+\Delta y,z,\theta,t_k) - \vec{B}_z(x,y-\Delta y,z,\theta,t_k)}{2\Delta y} - \frac{\vec{B}_y(x,y,z+\Delta z,\theta,t_k) - \vec{B}_y(x,y,z-\Delta z,\theta,t_k)}{2\Delta z}\right) + \frac{1}{3}\left[4\vec{E}_x(x,y,z,\theta,t_{k-1}) - \vec{E}_x(x,y,z,\theta,t_{k-2})\right] \tag{19}$$

$$\vec{E}_y(x,y,z,\theta,t_k) = \frac{2\Delta t}{3\varepsilon_0\mu_0}\left(\frac{\vec{B}_x(x,y,z+\Delta z,\theta,t_k) - \vec{B}_x(x,y,z-\Delta z,\theta,t_k)}{2\Delta z} - \frac{\vec{B}_z(x+\Delta x,y,z,\theta,t_k) - \vec{B}_z(x-\Delta x,y,z,\theta,t_k)}{2\Delta x}\right) + \frac{1}{3}\left[4\vec{E}_y(x,y,z,\theta,t_{k-1}) - \vec{E}_y(x,y,z,\theta,t_{k-2})\right] \tag{20}$$

$$\vec{E}_z(x,y,z,\theta,t_k) = \frac{2\Delta t}{3\varepsilon_0\mu_0}\left(\frac{\vec{B}_y(x+\Delta x,y,z,\theta,t_k) - \vec{B}_y(x-\Delta x,y,z,\theta,t_k)}{2\Delta x} - \frac{\vec{B}_x(x,y+\Delta y,z,\theta,t_k) - \vec{B}_x(x,y-\Delta y,z,\theta,t_k)}{2\Delta y}\right) + \frac{1}{3}\left[4\vec{E}_z(x,y,z,\theta,t_{k-1}) - \vec{E}_z(x,y,z,\theta,t_{k-2})\right] \tag{21}$$

$$\vec{E}_r\left(r,z,\phi,\theta,t_k\right) = \cos\left(\frac{\pi}{2}-\phi\right)\vec{E}_x\left(x,y,z,\theta,t_k\right) + \sin\left(\frac{\pi}{2}-\phi\right)\vec{E}_y(x,y,z,\theta,t_k) \quad (22)$$

$$\vec{E}_\varphi\left(r,z,\phi,\theta,t_k\right) = -\sin\left(\frac{\pi}{2}-\phi\right)\vec{E}_x\left(x,y,z,\theta,t_k\right) + \cos\left(\frac{\pi}{2}-\phi\right)\vec{E}_y(x,y,z,\theta,t_k) \quad (23)$$

$$\vec{E}_z\left(r,z,\phi,\theta,t_k\right) = \vec{E}_z(x,y,z,\theta,t_k) \quad (24)$$

where:
$\vec{E}_x(x,y,z,\theta,t_k)$ is the electric field at x-direction associated with the inclined lightning channel,
$\vec{E}_y(x,y,z,\theta,t_k)$ is the electric field at y-direction associated with the inclined lightning channel,
$\vec{E}_z(x,y,z,\theta,t_k)$ is the electric field at z-direction associated with the inclined lightning channel(vertical electric field),
$\vec{E}_r\left(r,z,\phi,\theta,t_k\right)$ is the electric field at r-direction(horizontal) due to inclined lightning channel,
$\vec{E}_\varphi\left(r,z,\phi,\theta,t_k\right)$ is the electric field at φ-direction due to inclined lightning channel,
$\vec{E}_z\left(r,z,\phi,\theta,t_k\right)$ is electric field at z-direction (vertical) due to inclined lightning channel,
$t_k = k\Delta t$.
Computational stability requires the condition specified in Equation (25). Note that, $\Delta x = \Delta y = \Delta z < \lambda_e/10$ where λ_e is the wavelength [16].

$$\Delta t \leq \frac{1}{c\times\sqrt{\frac{1}{(\Delta x)^2}+\frac{1}{(\Delta y)^2}+\frac{1}{(\Delta z)^2}}} \quad (25)$$

According to proposed algorithm, the current model (in this study MTLE model) has been entered into magnetic flux density calculations by $i(r', t-\frac{R(r')}{c})$ parameter in Equations (9) to (11). Therefore, the current model effect on the electric field calculations has been established indirectly through magnetic flux density values in Equations (19) to (21).

4. RESULT AND DISCUSSION

In this section, the proposed equation reflects on the return stroke current parameters that were obtained from Table 1. Likewise, the proposed method is validated via the data from three measured fields.

By the same token, new equations are corroborated by the data gathered from the measured fields from vertical lightning channel when the channel angle (θ) is assumed to be equal to zero. The magnetic flux density and the vertical electric fields due to an inclined lightning channel were estimated using TL, MTLE and MTLL models (Figures 7 and 8, respectively) by considering the current parameters obtained from Table 1 and a fixed return stroke velocity of $v = 1.3\times10^8$ m/s.

Figures 7 and 8 illustrate that the magnetic flux density values for three models are almost the same at close distance from the lightning channel. However, the simulated vertical electric field due to MTLE model has higher values than the other two models. On the other hand, by applying MTLE model as the current model, the effect of return stroke velocity observation point height on magnetic flux density and the vertical electric filed are taken into account as illustrated in Figures 9 and 10, respectively. It should be noted that in order to see the effect of observation point height, the velocity should be set at $v = 1.3\times10^8$ m/s.

As demonstrated in Figures 9 and 10, an increase in velocity results in an increase in the magnetic flux density values but a decrease in the vertical electric field values. Similarly, as the observation point height with respect to the ground increases, the magnetic flux density values boost up and the vertical electric fields decline. The magnetic flux density and the vertical electric filed behaviors versus the channel angle and observation point angle changes are shown in Figures 11 and 12, respectively.

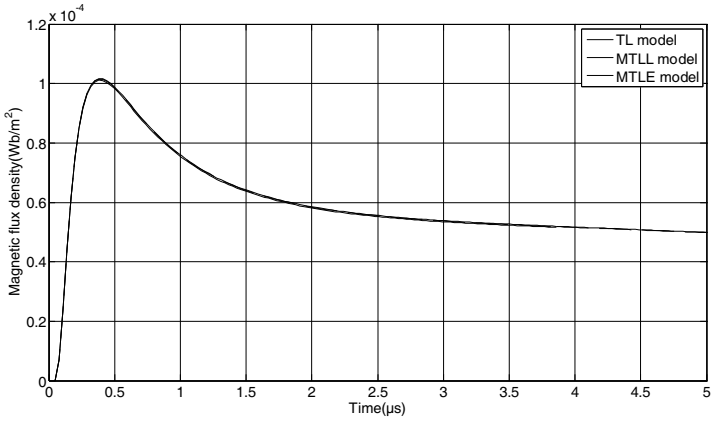

Figure 7. The Magnetic flux density for different important engineering models ($r = 15$ m, $\theta = 20°$, $\phi = 60°$, $z = 0$, $\lambda = 2000$ m, $H = 7000$ m, $v = 1.3 \times 10^8$ m/s).

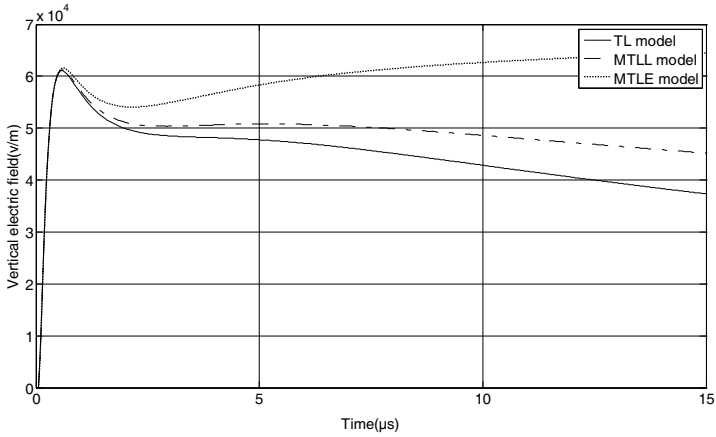

Figure 8. The vertical electric field for different important engineering models ($r = 15\,\text{m}$, $\theta = 20°$, $\phi = 60°$, $z = 0$, $\lambda = 2000\,\text{m}$, $H = 7000\,\text{m}$, $v = 1.3 \times 10^8\,\text{m/s}$).

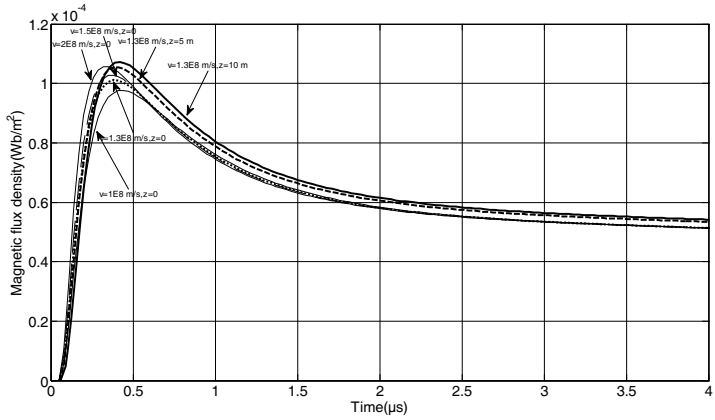

Figure 9. The Magnetic flux density behavior versus different return stroke velocities and observation point heights ($r = 15\,\text{m}$, $\theta = 20°$, $\phi = 60°$, $\lambda = 2000\,\text{m}$).

Figure 11 exhibits that by increasing the channel angle (θ) with respect to z-axis, the values of magnetic flux density fall. On the other hand, Figure 12 shows that the vertical electric field is directly depend on θ parameter and by increasing θ, the vertical electric field values are increased. In other words, whenever the observation point angle (ϕ) goes up to 90 degrees (at a constant value of θ), the values of vertical

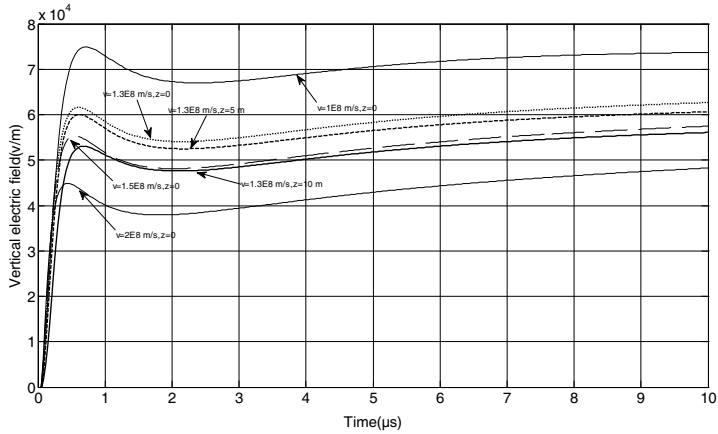

Figure 10. The vertical electric field behavior versus different return stroke velocities and observation point heights ($r = 15\,\text{m}$, $\theta = 20°$, $\phi = 60°$, $\lambda = 2000\,\text{m}$).

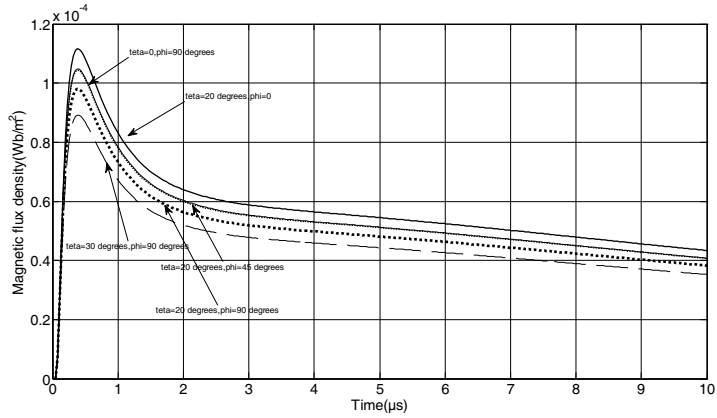

Figure 11. The magnetic flux density behavior versus different channel angles and observation point angles ($r = 15\,\text{m}$, $z = 0$, $\lambda = 2000\,\text{m}$, $v = 1.3 \times 10^8\,\text{m/s}$).

electric field and magnetic flux density drop, as shown in Figures 11 and 12, respectively. In addition, the proposed algorithm is validated using the three measured fields at different observation point angles (ϕ) with respect to y-axis as shown in Figures 13, 15 and 18 for $\frac{dE_z}{dt}$, E_z and B_φ respectively as the current parameters are obtained from Table 1 and the velocity is set at $v = 1.3{\times}10^8\,\text{m/s}$. Additionally, Figure 14 shows

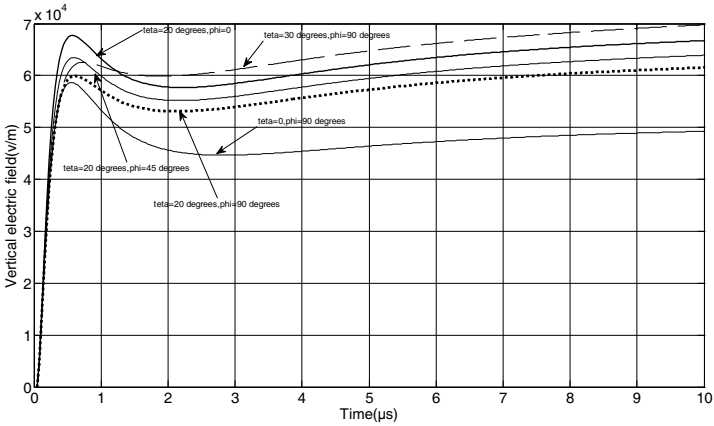

Figure 12. The vertical electric field behavior versus different channel angles and observation point angles ($r = 15\,\text{m}$, $z = 0$, $\lambda = 2000\,\text{m}$, $v = 1.3 \times 10^8\,\text{m/s}$).

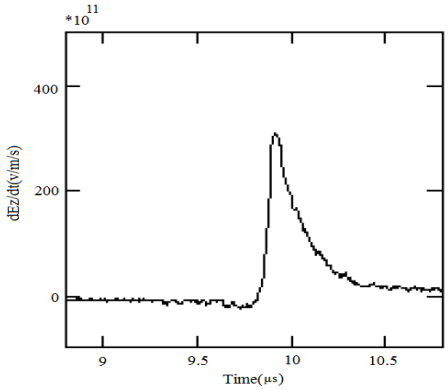

Figure 13. The measured $\frac{dE_z}{dt}$ ($r = 15\,\text{m}$, $z = 0$, $\phi = 135°$, $\theta = 20°$) [6].

a comparison between the measured derivative of vertical electric field and the time taken from Figure 13 with simulated results from inclined and vertical channels.

According to Figure 14, an increase is observed in the simulated values from inclined lightning channel with respect to similar field at vertical channel. These values are in line and close with each other comparing to measured fields. In addition, the simulated field from inclined channel is in agreement with the increase and decrease in time

based on measured field. Moreover, the measured vertical electric field at $\phi = 60^{\circ}$ (Figure 15) illustrates two parts for vertical electric field due to leader and return stroke (part (a)). So, the part of vertical electric field associated with return stroke indicated in part (b) is cut off from measured field The comparison between measured vertical electric field (Figure 15, part (b)) and simulated vertical electric field

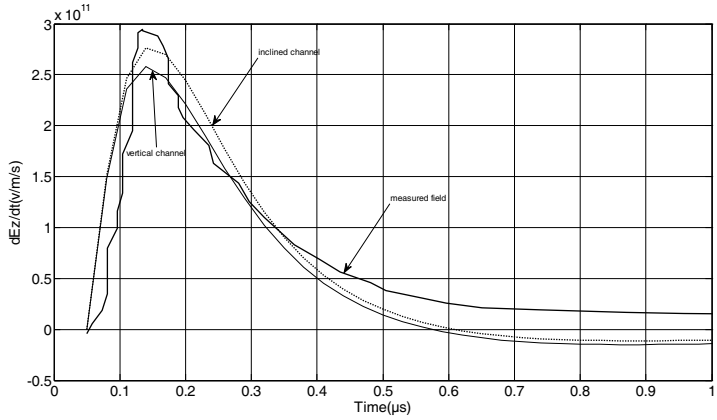

Figure 14. Comparison between simulated $\frac{dE_z}{dt}$ due to vertical and inclined lightning channels with measured values ($r = 15\,\text{m}$, $z = 0$, $\phi = 135^{\circ}$, $\theta = 20^{\circ}$, $v = 1.3 \times 10^8\,\text{m/s}$).

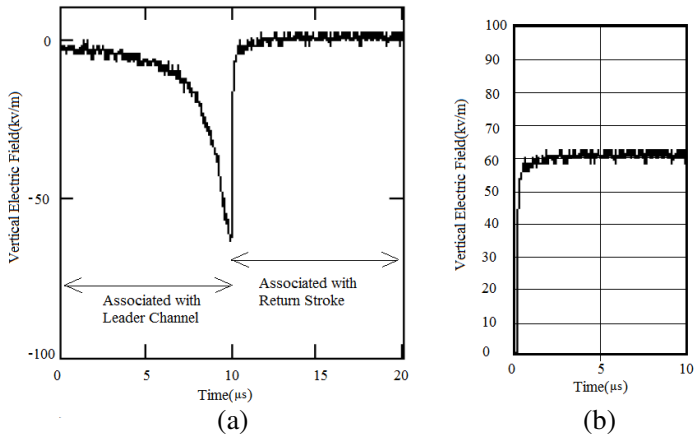

Figure 15. The measured vertical electric field ((a) associated with leader and return stroke, (b) associated with return stroke, $r = 15\,\text{m}$, $z = 0$, $\phi = 60^{\circ}$, $\theta = 20^{\circ}$) [6].

as a result of inclined and vertical lightning channel is exemplified in Figure 16, whilst the current parameters are obtained from Table 1.

Figure 16 demonstrates that the simulated vertical electric field is compatible with the inclined lightning channel in contrast to measured field. The vertical electric field values due to inclined channel have increased compared to similar fields associated with vertical channel. In other words, the vertical electric field is more effective in the coupling models and induced voltage values. Thus, evaluation of accurate vertical electric field values can be influential in predicting the induced voltage on the lines and setting appropriate protection levels on the power lines The simulated magnetic flux densities due to vertical and inclined channel are compared with those of the measured fields in Figure 18 when applying channel base current from Table 1 and are depicted in Figure 17. The figure reveals that the magnetic flux density due to inclined channel is lesser in value than in similar fields due to vertical channel; however, the difference between the values is negligible (See Figure 17). Likewise, the simulated results show an agreement between the two channels in contrast to measured field.

An algorithm is proposed that can support vertical lightning channel case when θ is set on zero. the simulated magnetic flux density, vertical and horizontal electric fields, respectively are shown in Figures 19, 20 and 21 using the proposed algorithm, while the observation point is located at 10 m height above ground surface and the radial distance from vertical lightning channel is equal 9 km as

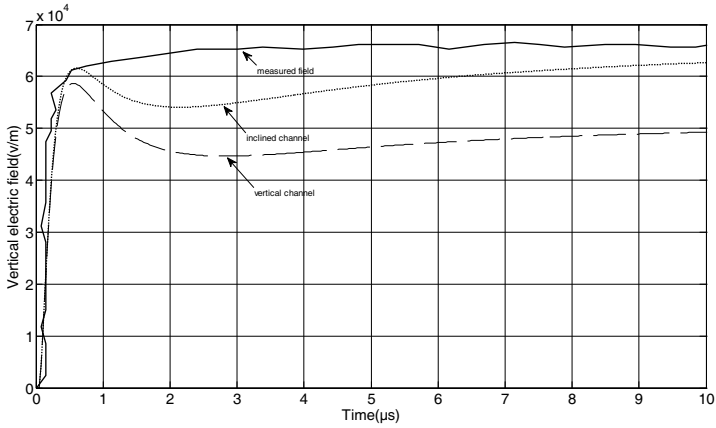

Figure 16. Comparison between simulated vertical electric fields due to vertical and inclined lightning channels with measured values ($r = 15\,\text{m}$, $z = 0$, $\phi = 135°$, $\theta = 20°$, $\lambda = 2000\,\text{m}$, $v = 1.3 \times 10^8\,\text{m/s}$).

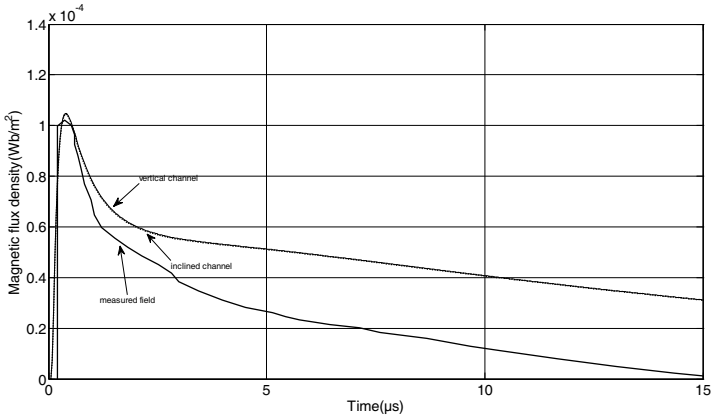

Figure 17. Comparison between simulated magnetic flux density due to vertical and inclined lightning channels with measured values ($r = 15\,\mathrm{m}$, $z = 0$, $\phi = 45°$, $\theta = 20°$, $\lambda = 2000\,\mathrm{m}$, $v = 1.3 \times 10^8\,\mathrm{m/s}$).

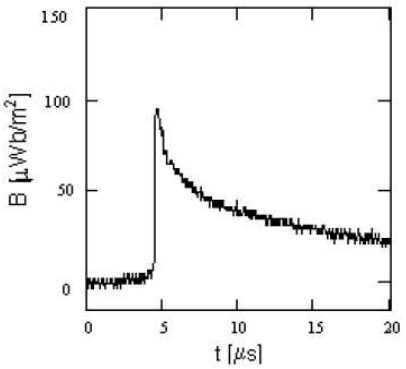

Figure 18. The measured magnetic flux density ($r = 15\,\mathrm{m}$, $z = 0$, $\phi = 45°$, $\theta = 20°$) [6].

expressed in the reference [16]. Note that, the current parameters are $\Gamma_{11} = 1\,\mu\mathrm{s}$, $\Gamma_{12} = 2\,\mu\mathrm{s}$, $\Gamma_{21} = 8\,\mu\mathrm{s}$, $\Gamma_{22} = 30\,\mu\mathrm{s}$, $i_{01} = 19.5\,\mathrm{kA}$, $i_{02} = 12\,\mathrm{kA}$, $n_1 = 2$, $n_2 = 2$, $v = 1 \times 10^8\,\frac{\mathrm{m}}{\mathrm{s}}$, $\lambda = 1500\,\mathrm{m}$, when the DU channel base current function and the MTLE current model are applied.

Therefore, the comparison between simulation results using the proposed algorithm and measured fields and other simulation results from the method in the reference [16] show that the proposed algorithms are in agreement. On the other hand, the proposed

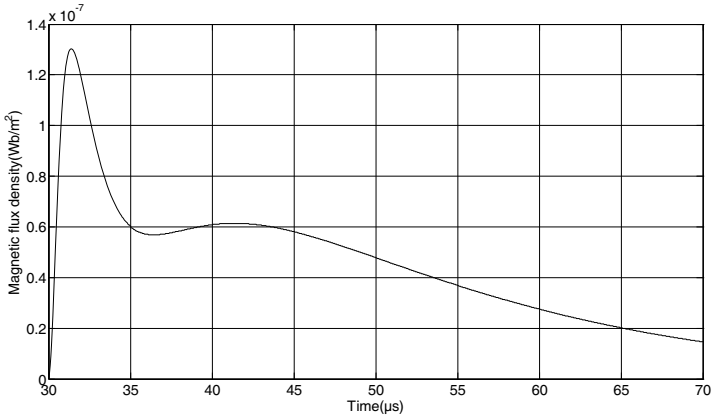

Figure 19. The simulated magnetic flux density ($r = 9000\,\text{m}$, $z = 10$, $\theta = 0^\circ$, $\lambda = 1500\,\text{m}$, $v = 1 \times 10^8\,\text{m/s}$).

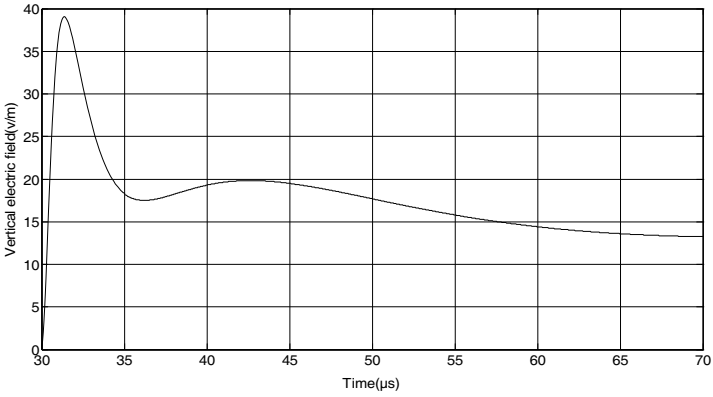

Figure 20. The simulated vertical electric field ($r = 9000\,\text{m}$, $z = 10$, $\theta = 0^\circ$, $\lambda = 1500\,\text{m}$, $v = 1 \times 10^8\,\text{m/s}$).

algorithm does not rely on observation point angle (ϕ) when it is used in vertical lightning channel basis. The proposed algorithm is more compatible with different coupling models while different electromagnetic fields components can be estimated in the time domain.

Figures 22, 23 and 24 show the radial distance (r), the observation point angle (ϕ) and the channel angle (θ) effects on the peak of electromagnetic field components generated by inclined lightning channel, respectively while the basic current assumptions are obtained

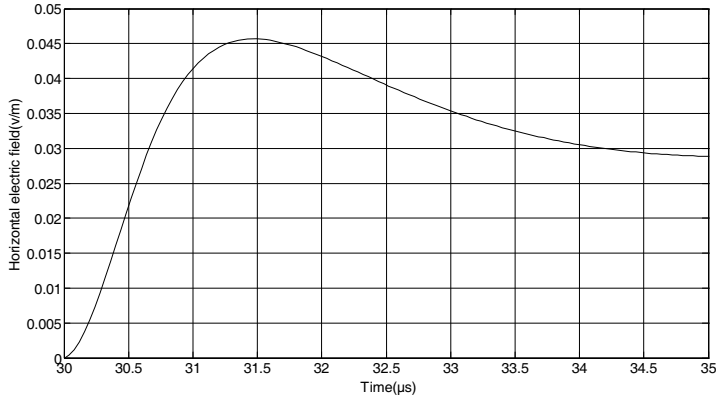

Figure 21. The simulated horizontal electric field ($r = 9000\,\mathrm{m}$, $z = 10$, $\theta = 0°$, $\lambda = 1500\,\mathrm{m}$, $v = 1 \times 10^8\,\mathrm{m/s}$).

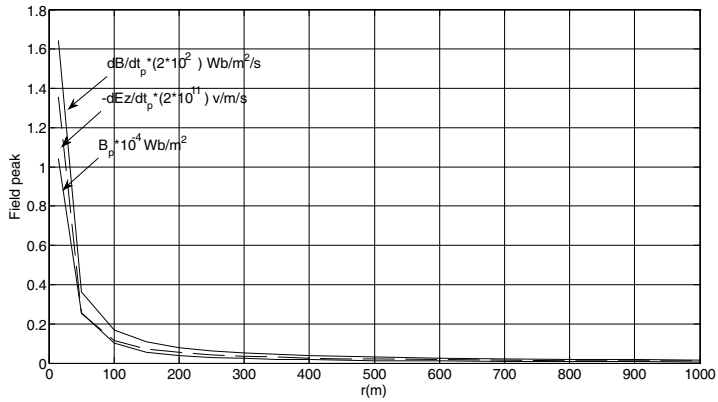

Figure 22. Radial distance effect on the electromagnetic fields peaks associated with inclined lightning channel ($z = 0$, $\phi = 45°$, $\theta = 20°$, $\lambda = 2000\,\mathrm{m}$, $v = 1.3 \times 10^8\,\mathrm{m/s}$).

from Table 1.

Figure 22 illustrates that by increasing the radial distance from lightning channel, peak of electromagnetic field components drop and this reduction in the near distance from lightning channel has a greater rate as compared to farther distances. Whilst Figure 23 shows that by increasing the observation point angle (ϕ) to 90 degrees, the peaks of electromagnetic fields have a downward trend until about 90 degrees when they are increased almost symmetrically with the first half. It is important to mention that the value of observation point

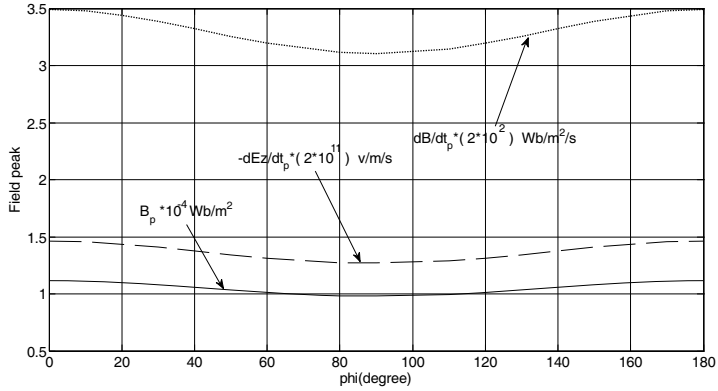

Figure 23. Observation point angle effect on the electromagnetic fields peaks associated with inclined lightning channel ($r = 15\,\text{m}$, $z = 0$, $\theta = 20°$, $\lambda = 2000\,\text{m}$, $v = 1.3 \times 10^8\,\text{m/s}$).

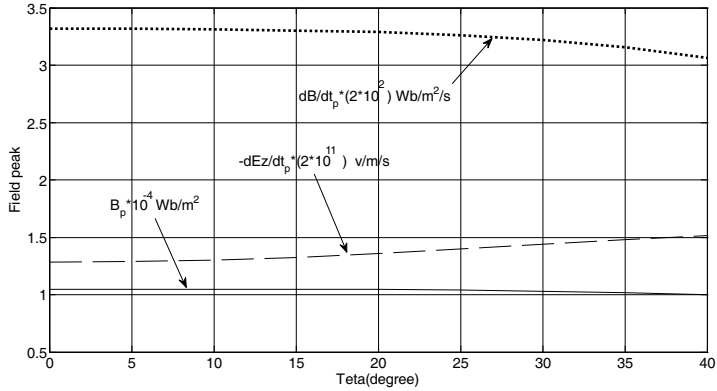

Figure 24. Channel angle effect on the electromagnetic fields peaks associated with inclined lightning channel ($r = 15\,\text{m}$, $z = 0$, $\phi = 45°$, $\lambda = 2000\,\text{m}$, $v = 1.3 \times 10^8\,\text{m/s}$).

angle is more effective on the value of x, y and $R(r')$ in Equations (9) to (11).

Figure 24 illustrates that by increasing the channel angle (θ), the peak values of magnetic flux density and dB/dt are reduced while the peak values of dEz/dt have a rising trend with opposite behavior compared to magnetic flux density.

In order to demonstrate the behavior of electromagnetic fields in the presence of a channel base current with higher decay-constant

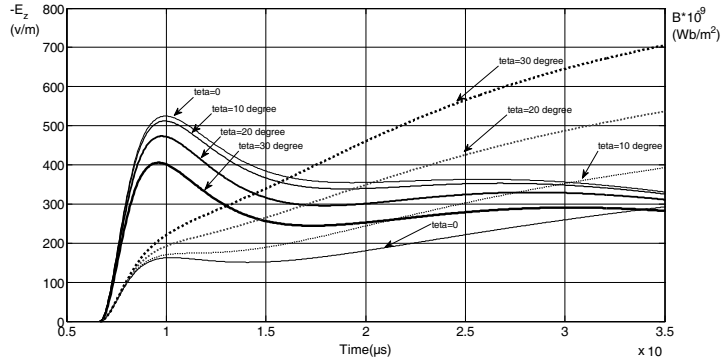

Figure 25. The simulated magnetic flux density (solid line) and vertical electric field (dot line) at different channel angles ($r = 2000\,\mathrm{m}$, $z = 10$, $\phi = 45°$, $\lambda = 1500\,\mathrm{m}$, $v = 1.5 \times 10^8\,\mathrm{m/s}$).

using proposed method, Figure 25 shows behavior of both magnetic flux density and vertical electric field at different channel angles. Note that, the current parameters are $\Gamma_{11} = 2\,\mu\mathrm{s}$, $\Gamma_{12} = 4.8\,\mu\mathrm{s}$, $\Gamma_{21} = 20\,\mu\mathrm{s}$, $\Gamma_{22} = 26\,\mu\mathrm{s}$, $i_{01} = 10.5\,\mathrm{kA}$, $i_{02} = 9\,\mathrm{kA}$, $n_1 = 2$, $n_2 = 2$, $v = 1.5 \times 10^8\,\frac{\mathrm{m}}{\mathrm{s}}$, $\lambda = 1500\,\mathrm{m}$ [16]. The results illustrate that by increasing the channel angle, the magnetic flux density is decreased while the vertical electric field is increased. Noted that the results at $\theta = 0$ are also validated with case 3 in reference [16].

In this study, a method was proposed that posse the following unique features:

1. The electromagnetic field components can be calculated directly at the time domain needless of employing Fourier transform, when a realistic channel base current function is applied (such as Heidler current function).
2. The proposed method can support different observation point angles (ϕ), while a number of previous methods just considered $\phi = 0$ which causes complications when simultaneous field values at several points are desired [24].
3. The accuracy of calculated fields can be increased by changing the values of Δt, Δx, Δy, Δz.
4. The proposed algorithm is compatible with other coupling models for the estimation of lightning induced voltage. Since the proposed method has FDTD structure, while the coupling models are usually introduced by two partial differential equations the FDTD method is just a common solution to coupling equations [1, 25–27]. In addition, the proposed method provides different

electromagnetic field components to be fed to various coupling models [1].

5. The proposed method is applicable for close and intermediate distances from the lightning channel.
6. The proposed method can be expanded to the lighting channels with the shape of a zigzag.

Further, the inclined lightning channel subject can be very beneficial in increasing the accuracy of the calculated induced voltage in the coupling models because of these two reasons:

1. Due to the inclined lightning channel, the vertical electric field values increased compared to the values of the vertical channel. Thus, it can be more effective on the shape of the induced voltage wave. Whereas, the lightning induced voltage is directly dependent on the vertical electric field values in some coupling models [1, 25, 28–30].
2. Due to inclined lightning channel, the observation point angle (ϕ) is an effective factor for the evaluation of electromagnetic fields. The radial distance between the charge along the lightning channel and various observation points at different observation point angles (ϕ) are different from each other; hence, the inclined lightning channel can be more effective on the calculation of lightning induced voltage on the power lines, while the coupling models rely more on the electromagnetic field components at different points along the power line [1, 25, 27, 31].

5. CONCLUSION

In this study, the electromagnetic fields due to inclined lightning channel were estimated using the 2nd FDTD method. An algorithm was proposed and then validated by three measured fields at a close distance from lightning channel. The results were compared with ones in simulated fields from vertical lightning channel. Likewise, the proposed equations were validated by measured fields from vertical lightning channel while the channel angle was assumed to be zero. Moreover, the effects of different geometrical and current parameters on the electromagnetic fields due to inclined lightning channel were discussed. It was capable of estimating the electromagnetic fields associated with the vertical lightning channel in the time domain. Besides, in order to bond to different coupling models, different electromagnetic fields components were available in the proposed method.

REFERENCES

1. Nucci, C. A., "Lightning-induced voltages on overhead power lines. Part II: Coupling models for the evaluation of the induced voltages," *Electra*, Vol. 162, 121–145, 1995.
2. Nucci, C. A., "Lightning-induced voltages on overhead power lines. Part I: Return stroke current models with specified channel-base current for the evaluation of the return stroke electromagnetic fields," *Electra*, Vol. 161, 75–102, 1995.
3. Rakov, V. and M. Uman, "Review and evaluation of lightning return stroke models including some aspects of their application," *IEEE Transactions on Electromagnetic Compatibility*, Vol. 40, 403–426, 1998.
4. Hill, R., "Analysis of irregular paths of lightning channels," *Journal of Geophysical Research*, Vol. 73, 1897–1906, 1968.
5. Hill, R., "Electromagnetic radiation from erratic paths of lightning strokes," *Journal of Geophysical Research*, Vol. 74, 1922–1929, 1969.
6. Uman, M., J. Schoene, V. A. Rakov, K. J. Rambo, and G. H. Schnetzer, "Correlated time derivatives of current, electric field intensity, and magnetic flux density for triggered lightning at 15 m," *Journal of Geophysical Research*, Vol. 107, 4160–4172, 2002.
7. Le Vine, D. and R. Meneghini, "Electromagnetic fields radiated from a lightning return stroke: Application of an exact solution to Maxwell's equations," *Journal of Geophysical Research*, Vol. 83, 2377–2384, 1978.
8. Le Vine, D. and R. Meneghini, "Simulation of radiation from lightning return strokes: The effects of tortuosity," *Radio Science*, Vol. 13, 801–809, 1978.
9. Nucci, C. A., G. Diendorfer, M. A. Uman, F. Rachidi, M. Ianoz, and C. Mazzetti, "Lightning return-stroke models with channel-base specified current: A review and comparison," *Journal of Geophysical Research*, Vol. 95, 20395–20408, 1990.
10. Heidler, F., "Analytische blitzstromfunktion zur LEMP-berechnung," *18th ICLP*, Munich, Germany, 1985.
11. Bruce, C. E. R. and R. H. Golde, "The lightning discharge," *Journal of the Institute of Electrical Engineering*, Vol. 88, 487–505, 1941.
12. Heidler, F., "Travelling current source model for LEMP calculation," *Proc. of the 6th Symposium and Technical Exhibition on Electromagnetic Compability*, Zurich, 1985.

13. Cooray, V., *The Lightning Flash*, IET Press, 2003.
14. Thottappillil, R., V. Rakov, and M. Uman, "Distribution of charge along the lightning channel: Relation to remote electric and magnetic fields and to return-stroke models," *Journal of Geophysical Research*, Vol. 102, 6987–7006, 1997.
15. Rakov, V., "lightning return stroke speed," *Journal of lightning Research*, Vol. 1, 2007.
16. Izadi, M., M. Z. A. Ab Kadir, C. Gomes, and W. F. Wan Ahmad, "An analytical second-FDTD method for evaluation of electric and magnetic fields at intermediate distances from lightning channel," *Progress In Electromagnetic Research*, Vol. 110, 329–352, 2010.
17. Izadi, M. and M. Z. A. Kadir, "New algorithm for evaluation of electric fields due to indirect lightning strike," *CMES: Computer Modeling in Engineering & Sciences*, Vol. 67, 1–12, 2010.
18. Schoene, J., "Analysis of parameters of rocket triggered lightning measured during 1999 and 2000 camp blanding experiment and modeling of electric and magnetic field derivatives using the transmission line model," MSC, University of Florida, 2002.
19. Zhou, X., "On independence completeness of Maxwell's equations and uniqueness theorems in electromagnetics," *Progress In Electromagnetic Research*, Vol. 64, 117–134, 2006.
20. Nevels, R. and C. S. Shin, "Lorenz, Lorentz, and the gauge," *IEEE Antennas & Propagation Magazine*, Vol. 43, 70–72, 2001.
21. Eslahchi, M. M. and E. Babolian, "On numerical improvement of Gauss-Lobatto quadrature rules," *Applied Mathematics and Computation*, Vol. 164, 707–717, 2005.
22. Kreyszig, E., *Advanced Engineering Mathematics*, Wiley-India, 2007.
23. Sadiku, M. N. O., *Numerical Technique in Electromagnetics*, CRC Press, LLC, 2001.
24. Song, T. X., Y. H. Liu, and J. M. Xiong, "Computations of electromagnetic fields radiated from complex lightning channels," *Progress In Electromagnetics Research*, Vol. 73, 93–105, 2007.
25. Paolone, M., C. A. Nucci, and F. Rachidi, "A new finite difference time domain scheme for the evaluation of lightning induced overvoltage on multiconductor overhead lines," *International Conference on Power System Transients (IPST)*, 596–602, 2001.
26. Paolone, M., C. A. Nucci, E. Petrache, and F. Rachidi, "Mitigation of lightning-induced overvoltages in medium voltage distribution lines by means of periodical grounding of shielding wires and of surge arresters: Modeling and experimental

validation," *IEEE Transactions on Power Delivery*, Vol. 19, 423–431, 2004.

27. Rachidi, F., "Formulation of the field-to-transmission line coupling equations interms of magnetic excitation field," *IEEE Transactions on Electromagnetic Compatibility*, Vol. 35, 404–407, 1993.
28. Borghetti, A., A. Morched, F. Napolitano, C. A. Nucci, and M. Paolone, "Lightning-induced overvoltages transferred through distribution power transformers," *IEEE Transactions on Power Delivery*, Vol. 24, 360–372, 2008.
29. Borghetti, A., J. Gutierrez, C. A., Nucci, M. Paolone, E. Petrache, and F. Rachidi, "Lightning-induced voltages on complex distribution systems: Models, advanced software tools and experimental validation," *Journal of Electrostatics*, Vol. 60, 163–174, 2004.
30. Gomes, C. and M. Z. A. Ab Kadir, "Protection of naval systems against electromagnetic effects due to lightning," *Progress In Electromagnetics Research*, Vol. 113, 333–349, 2011.
31. Rachidi, F., M. Rubinstein, S. Guerrieri, and C. A. Nucci, "Voltages induced on overhead lines by dart leaders and subsequentreturn strokes in natural and rocket-triggered lightning," *IEEE Transactions on Electromagnetic Compatibility*, Vol. 39, 160–166, 1997.